



Effect of coal maturity on CO₂-based hydraulic fracturing process in coal seam gas reservoirs



K.H.S.M. Sampath^a, M.S.A. Perera^{a,*}, D. Elsworth^b, P.G. Ranjith^c, S.K. Matthai^a, T. Rathnaweera^c, G. Zhang^c

^a Department of Infrastructure Engineering, Engineering Block B, Grattan Street, Parkville, The University of Melbourne, Victoria 3010, Australia

^b Energy and Mineral Engineering, G3 Center and EMS Energy Institute, Pennsylvania State University, University Park, PA 16801, USA

^c Department of Civil Engineering, Monash University, Clayton Campus, Victoria 3800, Australia

ARTICLE INFO

Keywords:

Coal seam
Hydraulic fracturing
Break-down pressure
Liquid CO₂

ABSTRACT

Hydraulic fracturing of deep coal seams is challenging due to both the complex processes involved in fracturing and the typically poorly defined characteristics such as natural cleat system, mineral-maceral distribution and strength parameters of the subsurface. This study evaluates the effectiveness of fracturing using liquid CO₂ as the propellant through observations of break-down pressures and the form of the induced fracture network in various ranked coals. Coal ranks are defined through a rigorous proximate analysis to determine the moisture, volatile matter, ash and fixed carbon contents of each coal type fractured. Fracturing experiments were conducted on 38 mm × 76 mm core samples, under fixed stress, temperature conditions (i.e. $\sigma_3 = 6$ MPa, $\sigma_1 = 8$ MPa and $T = 25$ °C). Break-down pressures are observed to increase with increasing coal maturity. Increasing rank or maturity identifies that the coal has been subjected to progressively higher pressures and temperatures, has gained proportionately higher strength and thus exhibits a higher break-down pressure. No direct relationship is observed between volatile matter content and either strength or break-down pressure. The collocation of acoustic emission (AE) hypocenters and mineral grain boundaries delineated by micro-CT imaging indicate preferred pathways for the propagation of fractures induced by liquid CO₂. Stiffness contrasts between mineral phases result in stress concentrations and localized weakness at grain-grain boundaries. The complex mineral distribution in coal accentuates such heterogeneity of weakness and may be the key feature promoting the evolution of a well distributed rather than localized fracture network. For low rank coal, hydraulic fracturing is least effective, as the fracturing process does not create a significant fracture network to enhance the permeability. This may result, since low rank coals are intrinsically weak due to their low carbon content and high moisture content allowing extensive fracturing to develop at only very low break-down pressures – minimizing damage. These observations emphasize the sensitivity of break-down pressures and the resulting complexity of fracturing to pressurization rates and coal rank – inferring important controls on these parameters for the safe and effective use, when fracturing with CO₂ as the propellant.

1. Introduction

The need for sustainable energy resources is rapidly expanding due to the rapid growth of population and the spectre of climate change. Exploration of alternative energy resources has become essential to fulfill an ever-increasing energy demand. One potential source of energy is extraction of unconventional gases, such as basin-centered gas, tight gas, coal seam gas (CSG) and shale gas [1]. The extraction of natural gas from low permeability unconventional reservoirs requires methods to improve access to the reservoir. ‘Hydraulic fracturing’ is one

such technique which has made gas extraction both feasible and commercially viable [2].

Hydraulic fracturing is defined as the injection of a pressurized fluid into a rock formation through a wellbore, to create a network of fractures as a pathway for the gas to move towards the wellbore [3]. Hydraulic fracturing is a well-accepted technique in gas extraction, particularly in low permeability reservoirs such as for coal and shale. For low-permeability unconventional reservoirs, horizontal wells with multi-staged hydraulic fractures are necessary to deliver an economic production [4]. The first experiment on hydraulic fracturing for well

* Corresponding author at: Department of Infrastructure Engineering, Room: B 209, Engineering Block B, Building 175, Grattan Street, Parkville, The University of Melbourne, Victoria 3010, Australia.

E-mail address: samintha.perera@unimelb.edu.au (M.S.A. Perera).

<https://doi.org/10.1016/j.fuel.2018.08.150>

Received 7 January 2018; Received in revised form 13 June 2018; Accepted 30 August 2018

0016-2361/ Crown Copyright © 2018 Published by Elsevier Ltd. All rights reserved.

stimulation was completed in 1947 and the technique was first introduced to the petroleum industry by the Stanolind Oil and Gas Company in 1949 [2]. Since then, hydraulic fracturing has become a routine and widespread technique and it is estimated that up to 80% of all natural gas wells in the next 10 years will be hydraulically fractured [1].

Hydraulic fracturing in coal seams is mainly associated with conventional water based techniques, which use water as the base fluid along with additives and proppants. Although, “conventional” fracturing with “slick-water” is generally simple and cost effective [5], it is sometimes no longer acceptable due to environmental impacts from constituent chemicals, water scarcity, and from poor fracture containment or performance [2,3]. The excessive usage of water may cause several social and environmental issues, including agricultural and residential issues due to depletion of the local groundwater table, high cost to dispose of and treat the contaminated flow-back water and localized low-level earthquakes due to uncontrolled fracture performance [6]. These significant issues associated with water-based hydraulic fracturing in coal seams have led to the exploration of the use of alternative non-aqueous fracturing fluids.

Of the various non-water based fracturing fluids, CO₂ has been identified as an effective option. Alpern et al. [7] showed that CO₂ based hydraulic fracturing has the ability to create more controlled and interconnected fracture networks, which significantly enhances the ultimate gas productivity. CO₂ as a fracturing fluid eliminates formation damage and the residual fracturing fluid [8]. Furthermore, studies have been extended on evaluating the possibility of combining CO₂ sequestration with CO₂-based gas recovery from tight gas reservoirs [9]. More importantly, it will significantly reduce the potential social and environmental issues caused by conventional fracturing fluids. For all of these reasons, it is necessary to understand the behavior of CO₂ in the rock mass, once it is injected through the wellbore. The flow behavior, fluid-rock mass interactions and storage mechanisms are some of the crucial factors which should be considered when evaluating a hydraulic fracturing project.

Coal seams are formed from partially decomposed vegetation that has undergone a process called ‘coalification’ over millions of years. Unlike other potential gas reservoirs, coal seam hydraulic fracturing is quite challenging due to a number of factors including: 1) mechanical complexity, 2) complex geometry of induced fractures, 3) high sensitivity of coal to the fracturing fluid and; 4) stress sensitive permeability of coal seams [10]. Coal can be categorized according to its various characteristics and the CO₂ flow behavior in each coal type is different. Coal mass strength, coal-CO₂ interactions and fracture mechanisms may vary according to the coal type and its composition. Accordingly, the hydraulic fracturing break-down pressure, fracture initiation and propagation, and induced fracture characteristics also vary. This implies that the characteristics of the targeted coal reservoir should be investigated and identified, and that hydraulic fracturing projects should be specifically designed and implemented, targeting the particular characteristics of the coal formation.

This study experimentally investigates the variations of CO₂-based hydraulic fracture characteristics in coals of various compositions. A high-pressure tri-axial loading apparatus has been developed to conduct the fracturing experiments on coal samples by simulating in situ reservoir conditions. Four coal types in the range of sub-bituminous to bituminous (according to ASTM classification [11]) have been selected for the study and all specimens were fractured under the same conditions with CO₂ as the fracturing fluid. A proximate analysis classifies the coal types by determining the moisture, ash, volatile and fixed carbon content in each specimen. The fracturing results are discussed relative to these categories. The break-down pressure, acoustic emission (AE) event locations and counts, and micro-CT analysis are used to evaluate and compare mechanisms of fracture initiation and propagation in each coal type.

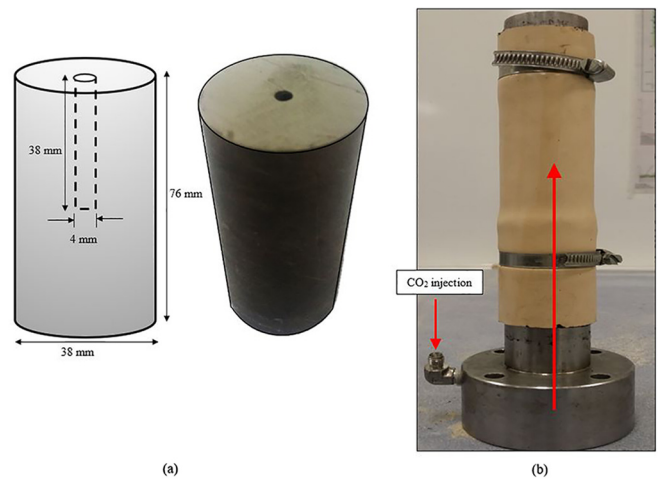


Fig. 1. a) prepared sample for fracture experiment; b) sample placement on the modified pedestal for CO₂ injection into the sample.

2. Experimental procedure

2.1. Sample preparation

The coal samples from each coal type were cored and cut with a diameter of 38 mm and a length of 76 mm using diamond coring and cutting machines available in the Deep Earth Energy Research Laboratory (DEERL) of Monash University. Both ends of the cored samples were ground to achieve smooth, flat, parallel surfaces using a face grinder to ensure a uniform stress distribution. The fracturing fluid was injected at a constant flow rate through a 4 mm diameter hole drilled halfway through at the middle of the sample (see Fig. 1(a)). The prepared sample was placed on a specially designed pedestal and the bottom was sealed off to prevent any CO₂ leaking during the fracture fluid injection. A nitrile membrane with 37.5 mm internal diameter and 3 mm wall thickness was used to cover the sample to prevent any damage from the confining oil (see Fig. 1(b)).

2.2. Modified rock tri-axial setup for CO₂ hydraulic fracturing

The high pressure tri-axial apparatus developed in the DEERL of Monash University is ideal for rock hydraulic fracturing using CO₂. The apparatus consists of four major parts: 1) pressure cell, 2) loading frame, 3) fluid pumping system and, 4) data acquisition system (see Fig. 2). The setup can deliver injection pressures up to 50 MPa, confining pressure up to 70 MPa, axial load up to 100 kN and temperature

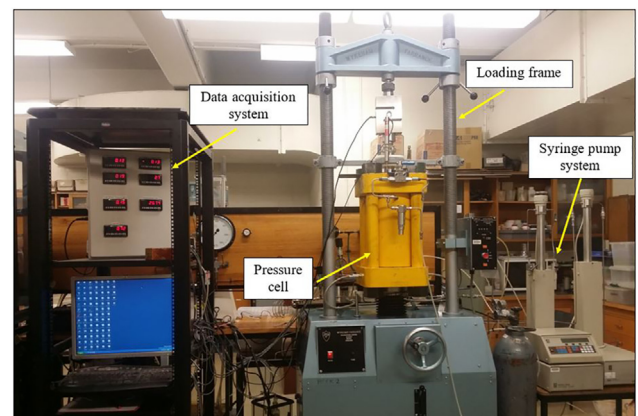


Fig. 2. Modified rock tri-axial setup used for CO₂-based hydraulic fracturing, indicating the four major components.

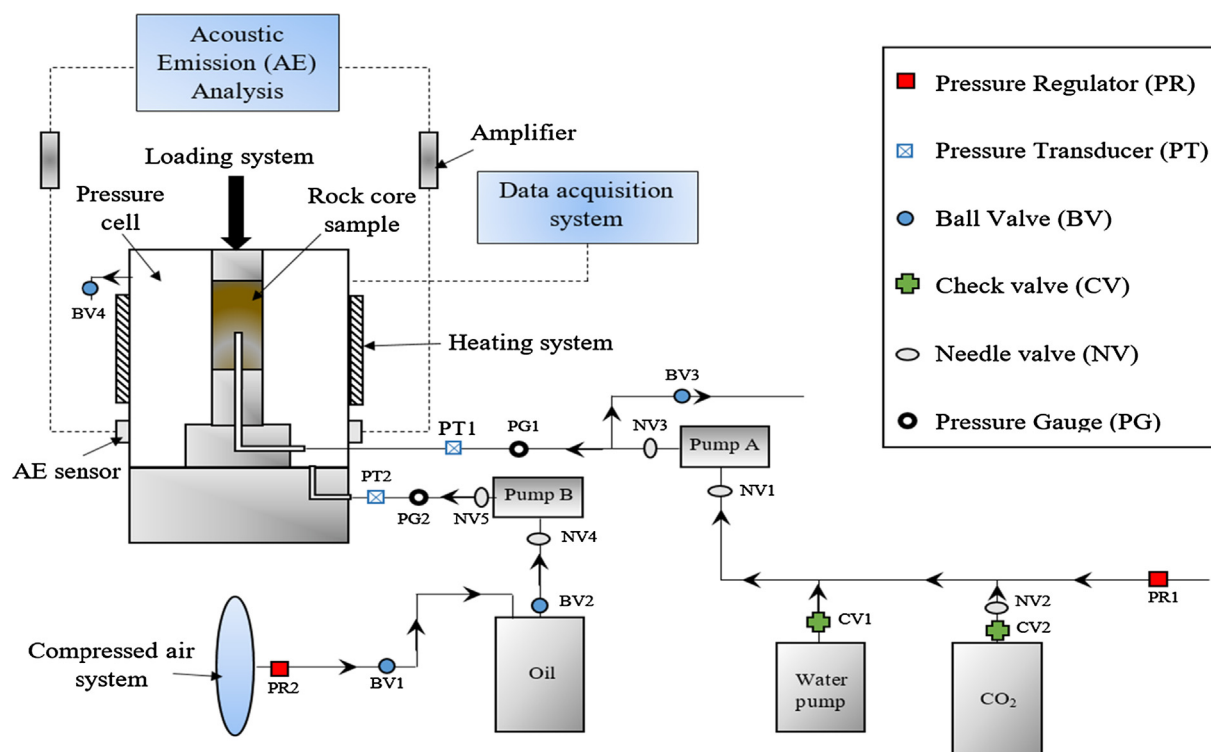


Fig. 3. Schematic diagram of the modified rock tri-axial setup, used for CO₂-based hydraulic fracturing.

up to 70 °C. As shown in the schematic diagram (see Fig. 3), two separate syringe pumps (capacity of 266 ml) were used to apply confining pressure and inject fluid into the sample. High pressure needle valves, ball and check valves suited for the maximum working pressure were used to fit the tri-axial cell. 6.35 mm NPT threading and 6.35 mm stainless steel tubes were used for all external connections, whereas 3.175 mm NPT threading and 3.175 mm stainless steel tubing and fittings were used inside the cell to create more space inside the cell. The cell was allowed to freely move up and down, when applying and releasing the vertical stress, respectively. The horizontal stress (σ_3) was provided by hydraulic oil and was maintained at a constant value by the syringe pump throughout the experiment. Theoretically, the induced fractures are perpendicular to the axis of least stress, regardless of the type of fracturing fluid [2]. Therefore, an additional vertical stress ($\Delta\sigma_1$) was given by the loading frame (i.e. $\sigma_1 > \sigma_3$), in order to create the fracture network in a vertical plane. Pressure transducers and pressure gauges were used in each inlet to continuously measure the applied pressure. The data acquisition system was capable of monitoring and recording the confining pressure, injection pressure, vertical load, vertical displacement and time at given intervals throughout the experiment.

2.3. Experimental process for CO₂-based hydraulic fracturing of coal

Once the prepared sample was placed on the pedestal, sealed off the bottom and covered with the membrane, the pedestal was mounted in the setup and the CO₂ inlet tube was connected to the pedestal. The pressure cell was lowered and sealed to prevent any oil leak during the experiment. The pressure cell was filled with hydraulic oil and the required confining pressure was provided and maintained at a constant value using the pump B (see Fig. 3). The required additional vertical stress was calculated considering the sample top area and was applied on the sample using the loading frame. For all the samples of this experiment series, a constant horizontal stress of 6 MPa and a vertical stress of 8 MPa were maintained. The stress environment was selected by considering four factors: 1) to represent a ground depth varying from

600 m to 1200 m, considering the bulk densities of the selected coal samples, 2) to maintain injected CO₂ at liquid state at break-down, 3) to prevent any damage to the samples during stress application and 4) to maintain a vertical fracture plane. Pump A, which has a capacity of 266 ml was completely filled with CO₂ from the CO₂ bottle, prior to the experiment to make sure that there was enough CO₂ in the pump to carry out the test. Once the setup was stable, the CO₂ was injected into the sample using the pump A at a constant flow rate of 90 ml/min. The injection flow rate was determined after a series of trial tests, in order to maintain a reasonable pressure development in the samples until the break-down. In fact, since CO₂ has a high compressibility, the pressure development is very slow, so that a higher injection pressure has to be maintained to achieve the break-down within a sensible time frame. The injection pressure was continuously monitored and a sudden drop down of the gradually increased pressure was observed at the break-down of the sample.

2.4. Acoustic emission (AE) analysis

The Acoustic emission (AE) technology was used to identify fracture initiation, propagation and failure in the coal samples during the each fracturing test. The AE system consists of a data acquisition system of PCI (peripheral component interconnection) 2-channel, which has a nominal resonant frequency of 500 kHz and a band-pass filter with a frequency range of 250–750 kHz. In each test, three sensors were attached to the pressure cell of the tri-axial setup and an electron wax was used on the sensors to obtain the same sensitivity. The amplifiers were used to magnify the low-frequency acoustic waves caused by the crack initiation and propagation process in the samples and were set to 40 dB to amplify the AE signals.

2.5. Micro-computed tomography (Micro-CT) analysis

Micro-CT analysis was performed on each coal specimen to analyse the variation of fracture distribution upon CO₂-based hydraulic fracturing. The whole sample (38 mm diameter and 76 mm length) was

Table 1
Imaging parameters and specification of the micro-CT instrument used in this study.

Scanning parameters	Specifications
Research facility	Australian Synchrotron imaging and medical beamline (IMBL) facility
Detector	Ruby with 150 mm lens and 20 μm screen
Sample size	38 mm (diameter) \times 76 mm (length)
Voxel size	16.7 μm
Acquisition time	20 min
Energy of X-ray	60 keV
Number of projections	3 segments per sample, 1800 projection per each segment
Detector to sample distance	1.4 m
Filter	none

carefully retrieved after the fracturing test and scanned in the Australian Synchrotron imaging and medical beamline (IMBL) facility. AVIZO image analysis software was used to visualize the fracture distribution. Imaging parameters and specification of the micro-CT instrument used in this study are given in Table 1.

2.6. Proximate analysis for coal classification

A proximate analysis was carried out to classify the coal samples according to their intrinsic characteristics. The proximate analysis of coal is formally defined by a group of ASTM test methods, which include the determination of moisture, volatile matter (VM), ash and fixed carbon (FC) contents [12]. The first three are determined by laboratory experiments and the fixed carbon content is found out by the difference. The detailed analysis procedure is described in references [12–15] with the corresponding ASTM standards. A summary of the determination of each content is briefly illustrated in Fig. 4.

3. Results and discussion

3.1. Proximate analysis results

Proximate analysis determines a group of components as a single generic material rather than individual components themselves [15]. Referring to ASTM standards, four basic component groups in a given coal sample are determined in proximate analysis, namely moisture, volatile matter, ash and fixed carbon. The moisture content is a combination of free and inherent moisture, which includes adsorbed water in the pores or on external surface of the coal, water of hydration of inorganic constituents and, dissolved water due to organic compounds' decomposition [14]. Volatile matter consists of gaseous substances like CO, H₂, CO₂, CH₄, N₂, O₂ and other hydrocarbons. The ash is generally composed of inorganic substances, which is obtained as residue after complete combustion of coal and consists of CaO, MgO, SiO₂, Al₂O₃ etc. Although, ash is often referred to as mineral matter, they are not identical [16]. However, since it is much easier to measure the ash content than mineral matter, ash content is often related to mineral matter in a particular coal sample. The Parr formula [17] is commonly used to calculate mineral matter content from the ash determination (see Eq. (1)). The fixed carbon content in a coal mass has not combined with other elements and is available in a free state. The fixed carbon content increases with the coal rank and is highest in anthracite [12]. Overall, the volatile matter and fixed carbon are the organic portion of the coal, whereas moisture and ash are extraneous impurities. Since the carbonaceous portion gives clear indication on coal maturity, it is often desirable to compare one coal with another by considering the carbonaceous or organic portion of coal, that is, to compare with volatile matter and fixed carbon contents [15].

$$MM = 1.08A + 0.55S \quad (1)$$

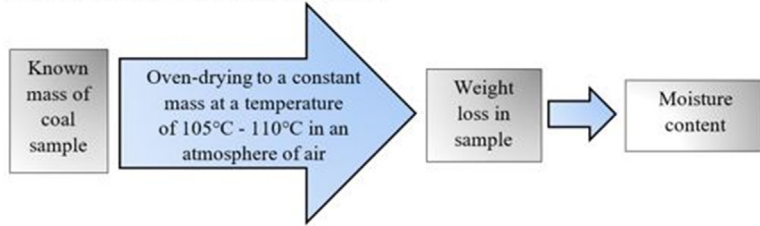
where, *MM* is the mineral matter content, *A* is the ash content and *S* is the sulfur content in coal.

This study has used four different coal types. The components of each type were determined by a rigorous proximate analysis and the results are given in Fig. 5. The results show that each specimen has different values for each component. However, the fixed carbon content is the most important component as it decides the rank and therefore the strength of the coal type. This should directly influence the break-down pressure and fracture propagation in the hydraulic fracturing process. The ASTM classification of coal by its rank is based on the moist mineral matter free (m.m.m.f) fixed carbon content and dry mineral matter free (d.m.m.f) volatile matter content [11]. Since ash content is directly related to the mineral matter content (see Eq. (1)) and assuming sulphur content is comparatively negligible, the m.m.f. content was approximated to ash free (a.f) basis in this study. As per the classification, the first three coal specimens belong to bituminous coal rank, where C-01, C-02 and C-03 are being medium volatile, high volatile and low volatile bituminous coals, respectively. The C-04 coal type should be a sub-bituminous coal as the fixed carbon content of it is considerable lower than that of others. C-01 specimen has the highest fixed carbon content of 65.4%, which indicates that it is the highest ranked coal type, among the four types used. The fixed carbon content is gradually decreasing with specimens C-01, -02, -03 and -04, indicating that the coal rank is decreasing from specimen C-01 to C-04. In fact, the deference of fixed carbon content in C-02, -03 and -04, with respect to C-01 are 8%, 18% and 42.6%, respectively. This shows that the fixed carbon content in C-04 specimen is considerably lower than that of others, thus should be a lower rank coal with a lower strength. Specimens C-01, -02 and -04 have very less ash contents (less than 10%), whereas specimen C-03 has a considerably higher ash content of 27.7%. According to the Parr formula, higher ash content is directly related to its higher mineral matter content (see Eq. (1)). This can be true, as the micro-CT image of specimen C-03 shows that it has a largely distributed mineral vein system (see Fig. 9(c)). C-04 type has a considerably large moisture content of 29.2%, which is another indication for a low rank coal. Each of these components play a critical role during the hydraulic fracturing process. The variations of break-down pressure, fracture propagation and distribution, and the possible scenarios are comprehensively discussed under following sections.

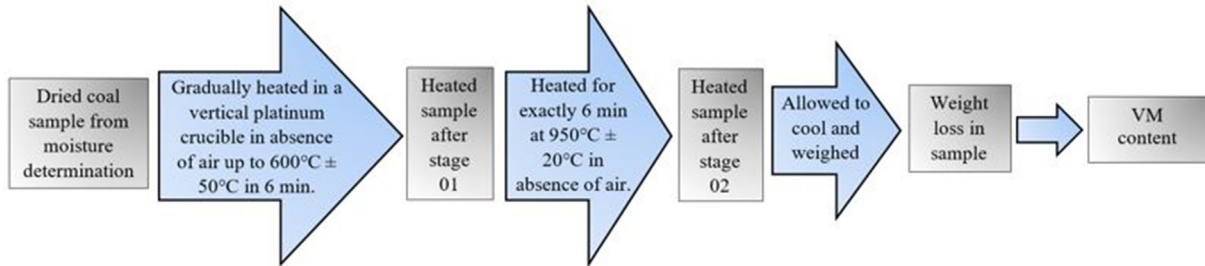
3.2. Variation of break-down pressure

The theoretical break-down pressure in hydraulic fracturing process has been explained by many researchers with considering various mechanisms. Some of the common break-down mechanisms include classical break-down model [18], the poro-elastic model [19], the point stress model [20] and shear failure model [21]. However, the actual break-down mechanism is somewhat more complex than the many proposed models as it depends on many parameters such as pressure rate, rock mass properties, fracture-fluid properties and wellbore size [22–24]. Based on the simplest theory proposed by Hubbert and Willis [18], it is expected that the break-down pressure will always be higher than the principal horizontal stress (confining pressure) (see Eqs. (2) and (3)). In fact, the theory suggests that the break-down pressure is equal to the combination of horizontal principal stresses and the rock tensile strength [18]. Therefore, the injection pressure has to overcome both the rock tensile strength and confining pressure to reach the break-down pressure (see Eq. (3)). The higher the confining pressure, the higher the break-down pressure [25]. Based on this conclusion, the confining pressure (σ_3) in each experiment of this study is maintained at 6 MPa to make sure that the CO₂ is always at liquid state at the break-down. The phase diagram of CO₂ illustrates that at temperature of 25 °C, CO₂ is at its liquid phase when the pressure is greater than 6 MPa (see Fig. 6). Therefore, in this study, it is expected that all the break-downs occur at pressures greater than 6 MPa while CO₂ is at its liquid state.

Moisture content (ASTM D3173)

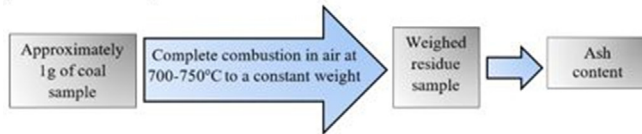


Volatile matter (VM) content (two-stage method) (ASTM D3175)



*If sparking is observed, the determination should be rejected and the test repeated until no sparking occurs either during the preliminary heating or during the 6 min period at 950°C.

Ash content (ASTM D3174)



Fixed carbon content (ASTM D5142)

$$\text{Fixed carbon content \%} = 100\% - \left(\text{Ash content \%} + \text{VM content \%} + \text{Moisture content \%} \right)$$

Fig. 4. A brief illustration of the determination of moisture, volatile matter, ash and fixed carbon content referred to the ASTM standards.

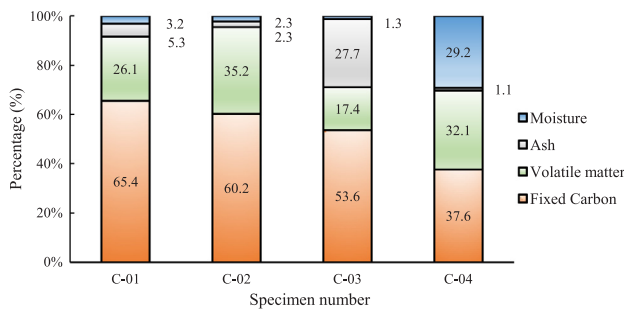


Fig. 5. Results from proximate analysis indicating the fixed carbon, volatile matter, ash and moisture content in each coal type.

$$P_b = (3\sigma_h - \sigma_H) + \sigma_t \quad (2)$$

$$P_b = 2\sigma_3 + \sigma_t \quad (3)$$

where, P_b is the break-down pressure, σ_t is the tensile strength of the rock mass, σ_h and σ_H are minimum and maximum principal horizontal stresses, respectively [18]. Note: in the tri-axial configuration used in the experiments, the horizontal stresses are applied hydraulically on core samples. Therefore, $\sigma_h = \sigma_H =$ confining stress (σ_3) as shown in Eq. (3).

To date, liquid CO₂ as a fracturing fluid has been shown numerous

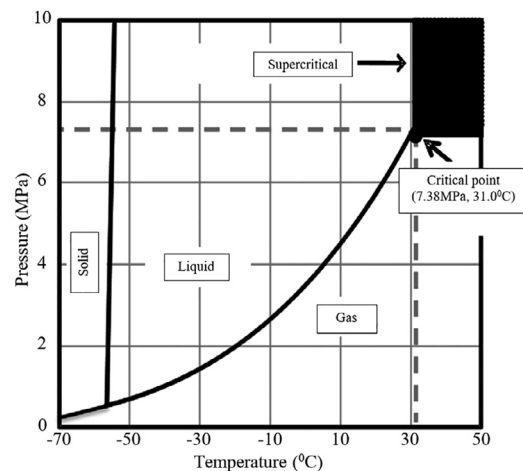


Fig. 6. Phase diagram of CO₂. Note that CO₂ is at liquid state at the temperature of 25 °C and pressures above 6 MPa [26].

advantages over conventional water based fracturing fluids. A number of experimental and numerical studies have been conducted on assessing the superiority of CO₂ as a fracturing fluid [26–29]. Being a low viscous fluid, liquid CO₂ has the ability to infiltrate through very small

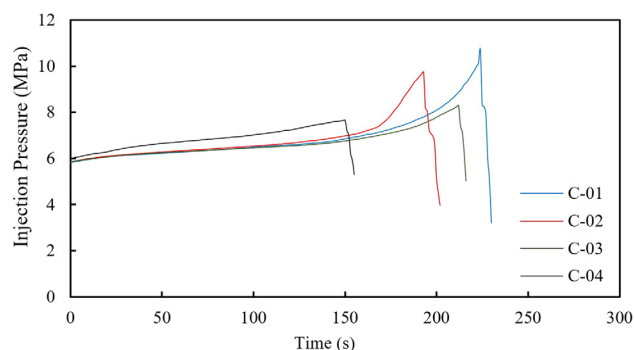


Fig. 7. Variation of injection pressure with time in each coal type until the break-down.

pores and thereby to induce a more distributed fracture network [26,30]. The enhanced fracturing mechanisms like the strong Joule-Thompson cooling effect associated with CO₂ would increase methane and other hydrocarbon production [28]. Despite all of these advantages, long term CO₂ injection in to the coal seam triggers other complex mechanisms including CO₂ adsorption induced coal matrix swelling [31] and coal seam strength reduction [32] and permeability loss. However, in this study, the break-down in each coal sample occurred in a very short time period (see Fig. 7), omitting any possible CO₂-induced coal matrix alterations in the samples.

Table 2 shows the CO₂ induced break-down pressures in each coal type under the same experimental conditions. As expected, all the break-down pressures are greater than the confining pressure of 6 MPa. This confirms that the break-down at each case occurred at the liquid phase of CO₂, because CO₂ becomes liquid at the temperature of 25 °C and pressures above 6 MPa (see Fig. 6). Fig. 7 shows the variation of injection pressure over the time for each specimen. With the injection of CO₂ into the samples, the pressure inside the sample increases gradually, followed by an exponential pressure increment before failure until the sudden pressure drop at the break-down. The higher the rate of pressure development before failure, the higher the break-down pressure. Since all the specimens follow the same trend, the time taken for the failure of each sample is proportional to the break-down pressure, with a slight reversal in specimen C-03. The only significant difference in specimen C-03, compared to the other coal types is the considerable ash content (27.7%), which represents a higher mineral matter content (see Fig. 5). The possible reason for the delayed break-down of this sample can be explained by considering the acoustic emission (AE) analysis. According to the AE results (see Fig. 10(c)), the corresponding sample has undergone a considerable period of stable fracture propagation before ultimate break-down. Unlike other samples, specimen C-03 does not exhibit unstable fracture propagation during the fluid injection. According to Ranjith et al. [33], the unstable fracture propagation period is the stage that creates a significant damage in the rock mass, which readily leads to failure. Absence of unstable fracture propagation has led the particular sample to a more controlled, stable and slow fracture propagation with a comparatively higher elapsed time period. This can be confirmed with the corresponding micro-CT image data. As illustrated in Fig. 9(c), the particular coal type has a complex mineral phase distribution, introducing a large heterogeneity to the

Table 2

Variation of break-down pressure in each coal sample under the same experimental conditions.

Specimen no	Experimental conditions	Break-down pressure (MPa)
C-01	Horizontal stress (σ_3) = 6 MPa,	10.71
C-02	Vertical stress (σ_1) = 8 MPa,	9.75
C-03	Constant flow rate = 90 ml/min.	8.3
C-04		7.65

sample. Thus, the weaker boundaries, interconnecting coal-mineral phases has also been distributed throughout the sample, resulting in a well distributed fracture network during the fracturing process. This has obviated the sample failure through one extensive fracture plane, which in turn caused a more stable and delayed break-down.

Since, the carbonaceous portion (i.e. volatile matter and fixed carbon contents) gives a clear idea about the coal maturity, it is necessary to compare any property of one coal with another by considering the carbonaceous portion of coal. Therefore, the break-down pressure of each coal type is compared with others, with respect to its fixed carbon and volatile matter content. However, the moisture content and ash content have often been used to reach important conclusions based on the experimental results.

According to Fig. 8(a), there is a direct relationship between break-down pressure and the fixed carbon content. In fact, the break-down pressure increases with respect to the fixed carbon content. Fixed carbon content is a direct indication of the rank of the coal [12]. The higher the fixed carbon content, the higher the coal rank. It is well-known that high rank coal is stronger, except for few unique cases like coal with dense natural cleat system, etc. This means that for the intact coal samples used for this study, the fixed carbon content has imparted a higher strength to the particular coal type, which in turn results in a higher break-down pressure. All the developed break-down models suggest that break-down pressure is a function of rock strength [18–20]. This is congruent with the observed results, as the high fixed carbon content results in a high strength in the sample, resulting in a higher break-down pressure. However, importantly, the variation of break-down pressure with fixed carbon content is non-linear (see Fig. 8(a)). For example, from samples C-04 to C-03, the fixed carbon content has been increased by 42.7%, whereas the break-down pressure increased only by 8.5%. Conversely, from samples C-03 to C-02, the fixed carbon content has been increased only by 12.2%, while the break-down pressure increased by 17.5%. This non-linear variation implies that fixed carbon content is not the only fact that affects the strength and the break-down of the sample, but rather the overall composition of coal type. For example, sample C-04 has the lowest fixed carbon content of 37.6% as well as the highest moisture content of 29.2% (moisture content of all the other coal types are less than 4% (see Fig. 5)). Higher moisture content in coal can reduce the strength due to the effect of softening. The interaction between water molecules and clay mineral affects the grain-to-grain contact and reduces the bond energy of the pore structure [34]. The coal structure is rearranged as the moisture forms hydrogen bonds with adsorbed water molecules and different other chemical constituents in mineral and maceral components, which in turn affects the coal strength [35]. The swelling effect induced by moisture adsorption can also reduce the coal strength, due to decreased capillary pressure, enlarged and relaxed volume, and stress concentration caused by differential swelling [36]. Thus, the significant moisture content may be another reason for a lower break-down pressure.

Fig. 8(b) illustrates the variation of break-down pressure with volatile matter content. The nonlinear trend between volatile matter content and the break-down pressure shows no simple relationship between each other (see Fig. 8(b)). This is quite agreeable, as the volatile matter content consists of a number of components, including gaseous substances and different hydrocarbons. A high volatile matter content does not always imply a higher strength since, different substances yield strengths at different levels in the sample. Without knowing the exact composition that contributes to the total volatile matter content and to the ultimate strength, it is difficult to establish a relationship with the break-down pressure. Therefore, the fixed carbon content is the best way to interpret the break-down pressure with respect to the coal type. However, it should be noted that the excessive presence of other substances can also alter the coal mass strength significantly, causing unpredicted break-downs during the operation.

When the overall results are considered, it can be seen that all the break-down pressures corresponding to all coal types are in the range of

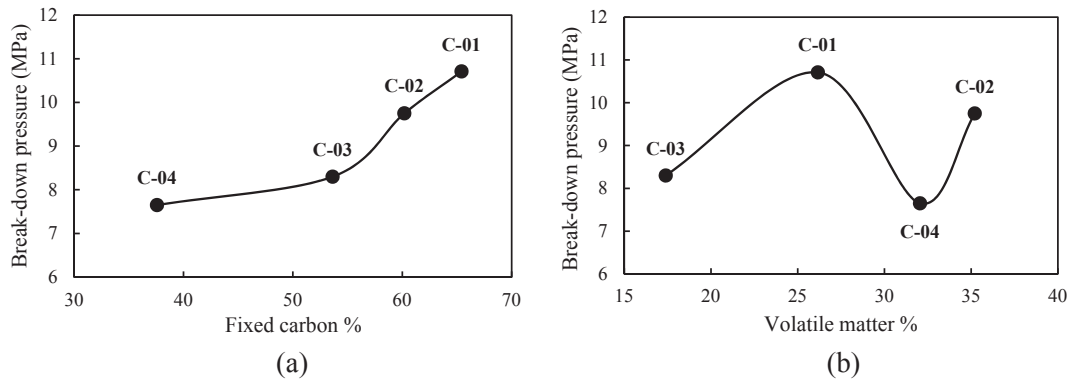


Fig. 8. Variation of break-down pressure of each coal type with; a) fixed carbon content and b) volatile matter content.

7 MPa to 11 MPa (see table 2). The increment of break-down pressure with respect to fixed carbon content (or rank) implies that the coal break-down pressure is a function of rock strength, because the higher the rank, the higher the coal strength. However, based on classical theory [18], for a confining pressure (σ_3) of 6 MPa, the break-down pressure should be higher than at least 12 MPa ($2\sigma_3$) (see Eq. (3)), because the model is based on the combination of horizontal principal stresses and the rock tensile strength. But all the results show lower break-down pressures than the predicted classical break-down pressures, which depicts the complexity of the actual break-down process. Number of numerical and experimental studies done on hydraulic fracturing using different fluids in various rock types support the fact that experimental results are mostly lesser than the theoretical ones [26,37,38], due to the assumptions using in the theoretical derivations. The overall lower break-down pressures than the predicted theoretical ones imply that the actual break-down phenomena and the fluid flow behavior through rock mass is much complex than the theoretical predictions, especially, when using non-water based fracturing fluids like liquid CO₂ and, when fracturing sensitive and heterogeneous rock formations like coal.

Theoretically, the stress alteration in a rock mass upon fracture fluid injection can be divided into three components, namely, 1) in-situ total stress field (S_0^i) due to the two horizontal principal stresses, 2) total stress developed due to injection pressure of fracturing fluid in wellbore (S_0^j) and, 3) total stress developed due to pore pressure distribution through the rock mass (S_0^p). The third stress component is often neglected in several theoretical models, due to its complexity. As shown in equation (4), the third stress component (S_0^p) is a function of pore pressure distribution ($p(r, t)$) at constant pressurization rate (C), distance from the wellbore (r), Biot's poro-elastic co-efficient (α) and rock Poisson's ratio (ν) [19]. The pore pressure distribution ($p(r, t)$), is again a function of both rock and fluid properties (see Eqs. (5) and (6)). Therefore, the magnitude of induced third stress component can be varied due to both rock and fluid properties, resulting in different break-down pressures. In the case of classical break-down theory, it is assumed that the rock formation is impermeable and break-down occurs at well bore wall. Therefore, the fluid flow beyond the well bore has not been considered and the actual effect of third stress component has been omitted in the theory. This can be true for cases, in which aqueous fluids (basically water) are being used as the fracturing fluid for hydraulic fracturing in very low permeable reservoirs. When using an aqueous medium as a fracturing fluid, it is difficult for the fluid to effectively penetrate into pores for a certain depth, especially in reservoirs with very low permeability. The fluid is therefore, unable to form a zone of high pore pressure. However, in the case of liquid CO₂, the influence of pore pressure on break-down pressure cannot be neglected because the percolation effect is so strong in liquid CO₂ due to considerably low viscosity and low surface tension [37,39]. When using liquid CO₂ for coal hydraulic fracturing, injecting liquid CO₂ penetrates

through the interconnected pores into coal from drill hole, and the liquid CO₂ penetration causes an additional tangential stress in compression around the wellbore [6]. This induced additional stress component due to pore pressure distribution, contributes to exert more pressure on the rock mass, so that a comparatively lower injection pressure is enough to overcome the rock break-down pressure. Based on this theory, number of theoretical and numerical studies have been done on understanding the complex behavior of low viscous fluids in reservoirs during the hydraulic fracturing process, which can create additional stress fields causing a low break-down pressure [20,38,40].

$$S_0^p = \frac{\alpha(1-2\nu)}{r^2(1-\nu)} \left[\int_{r_w}^r p(r, t) r dr - p(r, t) r^2 \right] \tag{4}$$

$$p(r, t) = C \int_0^t f(r, s) ds + P_0 \tag{5}$$

where;

$$f(r, t) = 1 + \frac{2}{\pi} \int_0^\infty \exp(-ku^2t) \times \left[\frac{J_0(ur)Y_0(ua) - Y_0(ur)J_0(ua)}{J_0^2(ua) + Y_0^2(ua)} \right] \frac{du}{u} \tag{6}$$

$k = k_r/\mu\eta\beta$, k_r is the rock permeability, μ is the fluid viscosity, η is the rock porosity, β is the fluid compressibility and J_0 and Y_0 are the Bessel functions of the first and second kind of order zero, respectively [20].

3.3. Fracture propagation and distribution in each coal type

The fracture initiation, propagation and the characteristics of the induced fracture network (fracture density, direction, fracture aperture, etc.) can be varied with different parameters. The fracture fluid properties, rock formation properties like composition and heterogeneity, pressurization rate are some of the key parameters that govern the induced fracture network. Since, all the other parameters, including the fracture fluid properties and fluid injection rate are the same in this study, the variation of the fracture network should primarily depend on the coal type and its composition. In this study, the combined results of the two methods, namely micro-CT image analysis and acoustic emission (AE) analysis have been used to clarify the fracture propagation and characterize the induced fracture network.

X-ray micro-computed tomography (micro-CT) is a technique that uses high-resolution three-dimensional X-ray images to analyse various geological materials [41]. The micro-CT image analysis has been often used by many researchers to visualize, quantify and differentiate the characteristics of fracture networks induced by different fracturing fluids [26,37]. The individual analysis of favourable sections in the coal sample, such as pores, fractures, minerals, macerals can be done by micro-CT technique as it has the capability of providing higher quality 3D images allowing for digital isolation and visualization [42]. The grey-scale difference of the scanned images allow to isolate the required

component of the coal sample. The colour variation or the grey-scale of a scanned image depend on the density of the particular component being scanned. The higher the density, the higher the brightness of the corresponding image section. For an example, low attenuation coefficients (grey-scale values) can be observed where a fracture exists. This is due to the density deficit caused by the lower density of the air-filled fractures than adjacent coal matrix regions [43]. Based on this key advantage, full scale scanning of 38 mm × 76 mm core samples have been carried out in this study to characterize the propagated fracture network. However, when using micro-CT images of full scale samples, it is difficult to visualize and accurately measure the micrometre-sized fracture apertures. This is because the sample size limits the maximum resolution of the scanning and the fracture apertures usually exist near the resolution limit. To overcome this limitation and to visualize a reasonable portion of the induced fracture network, image analysis software (AVIZO) has been used to highlight the induced fracture network (see Fig. 9). It should be noted that the discontinuity of some of the fractures shown in Fig. 9 may be caused by the lower resolution used for the full scale scanning of the samples, which has limited the caption of some of the thinner sections of the fracture network.

Any rock type subjected to external loading, leads to changes in the rock structure by closing or, initiating and propagating new micro fractures [44]. Acoustic waves represent the dynamic transport of strain energy released during this process. The spontaneously generated acoustic signals provide indirect information of micro-cracking such as fracture density, initiation time, direction of fracture propagation and induced fracture aperture. Monitoring the acoustic emission (AE) count during the fluid injection is a well-accepted method to analyse the fracture initiation, propagation and break-down. Many researchers have used this method to interpret the crack generation process in rock masses being subjected to hydraulic fracturing process [26,40,45]. The cumulative AE count released during the fracturing process helps to identify three main stages of the overall process, which are 1) crack closure, 2) stable crack propagation and 3) unstable crack propagation [33]. Depending on rock mass properties, it takes some time to initiate the first crack in an intact rock sample upon fluid injection. No AE count can be observed during this period and the rock mass is considered to be at its crack closure stage. The very first AE event indicates crack initiation and its location. The stable crack propagation period begins with the first AE hit and the AE energy is gradually released during this stage. The further injection of fluid through the wellbore results in unstable crack propagation. This is exhibited by an exponential increase in the energy release. The rock mass can undergo a significant damage during this stage until the eventual break-down. Referring this interpretation, in this study, the cumulative AE energy has been measured from fluid injection until break-down and is plotted with elapsed time (see Fig. 10). Each trend is used to identify fracture initiation, propagation and break-down, upon the injection of the fracturing fluid.

Fig. 9 illustrates that fracture initiation and propagation occurred from the drill hole upon CO₂ injection. Depending on the density variation of each component, the different compositions of the coal mass can be clearly differentiated as explained in the figure caption (see Fig. 9). Overall, the induced fracture network can be categorized as; (A) primary cracks initiated from the borehole, (B) secondary cracks parallel to or connected in parallel to the primary crack and, (C) secondary cracks perpendicular to the primary crack. Among them, the primary crack starting from the wellbore can be seen as the most extensive and widest crack. This is quite clear, because the highest pressure is always exerted on the wellbore wall during fracture fluid injection. However, due to the existing low viscosity and low surface tension of liquid CO₂, it has the potential to flow through the induced primary cracks and the natural interconnected pore network, creating secondary cracks both parallel and perpendicular to the primary cracks.

As apparent in Fig. 9(a) and (b), primary fractures always tend to propagate parallel to mineral grain boundaries rather than crossing

them. In fact, in Fig. 9(b), the primary crack has propagated along the interconnections between coal-mineral phases. In simple theory, fractures always tend to generate perpendicular to the axis of the least principal stress and propagate along the weakest path. This suggests that in the first two cases, the weakest path should be along the phase boundaries, which might due to the existing comparatively weaker interconnection. Studies show that the low viscous fluid induced cracks propagate mainly along the grain boundaries of constituent minerals, exhibiting a shear dominant fracturing mechanism [26]. Amann et al. [46] showed that a crack aligns as a boundary crack once it reaches a boundary of a mineral. It follows the stiffness contrast generated by the different elastic properties between the rock mass and mineral phase. Since, the boundaries of two components with different stiffnesses generates a plane of weakness, cracks can propagate along these boundaries. Furthermore Ündül et al. [47] showed that an increase in elastic moduli of individual minerals is more important than the overall elastic modulus of the rock mass, and can cause this type of boundary cracks.

Conversely, Fig. 9(c) shows a well distributed fracture network, which is initiated from the wellbore and spreads in every direction, indicating the distribution of the fracturing fluid. Unlike specimens C-01 and C-02, there is no favorable weak path for the fracturing fluid to flow along, generating a simple fracture network. The corresponding specimen (C-03) exhibits a much higher complexity in phase distribution, where the mineral phase has been distributed in every direction, covering a large portion of the coal mass. This observation may be related with its high ash content (27.7%) that indicating a high mineral matter content (see Fig. 5). The complex distribution of mineral phase has introduced a large heterogeneity to the sample, which has caused the development of a complex fracture network. In fact, the mineral-maceral interconnected boundaries have proven to be weaker than mineral or maceral phase itself, therefore the well distributed mineral vein system introduces weaker areas throughout the whole coal mass, eliminating any preferential weaker pathways for the fracture propagation. Thus, fractures tend to propagate in every direction following the heterogeneous distribution of weaker pathways, rather than failing the coal mass through a specific fracture plane with an extensive single fracture. However, if the constituent minerals contain preferential pathways that were generated during the tectonic history of the rock, the cracks may propagate along that preferential pathway, rather than following the mineral grain boundaries [46,47]. If the stresses generated by the pressurized fracturing fluid is sufficiently high, the crack can penetrate into the mineral phase, even into those with very high elastic moduli [46]. Nevertheless, the fracture distribution through the mineral phase cannot be explained accurately without knowing the exact mineral constituents contained in the mineral phase and their corresponding mechanical properties.

The cumulative AE count generated during fracture propagation suggests that sample C-03 has undergone a longer stable fracture propagation (see Fig. 10(c)). In fact, unlike other specimens, the sample does not show any unstable fracture propagation. The unstable fracture propagation period is that which causes irreversible damage to the rock formation, causing sudden failure [33]. Absence of unstable fracture propagation suggests that the sample has been subjected to a more controlled fracture propagation until the eventual break-down, upon the fracture fluid injection. This might be the possible reason for the delayed break-down described in Section 3.2. Thus, it can be concluded that due to heterogeneous distribution of mineral grain boundaries and weaker interconnecting areas, the fluid pressure applied through the wellbore has created a more dense fracture network in every direction. The well-distributed fracture network has allowed the fracturing fluid to flow in many directions, preventing a large pressure being focused at one particular point. This has obviated the sample break-down along one major extensive fracture and has minimized the uncontrolled fracture propagation along one direction, which in turn caused a more controlled and delayed break-down.

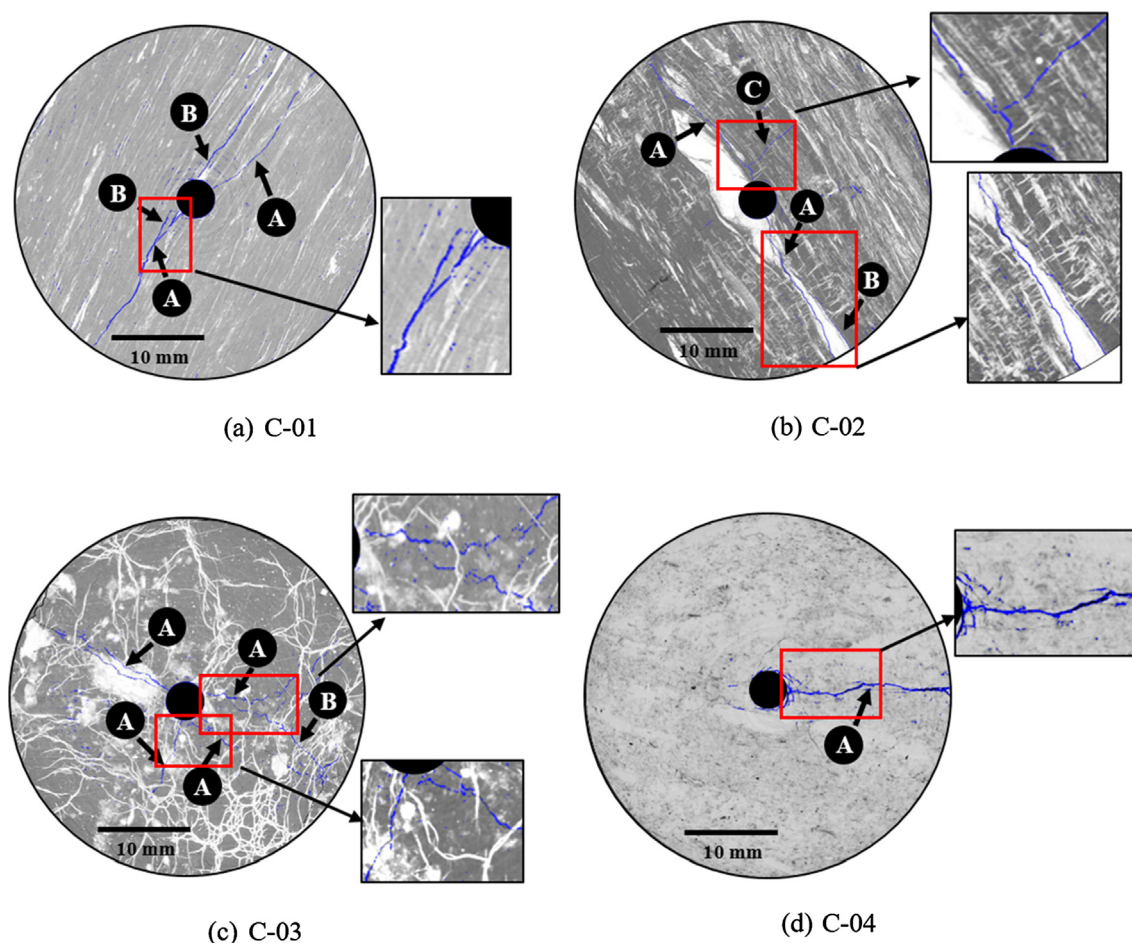


Fig. 9. Micro-CT images of fractured samples, indicating the fracture distribution from the borehole. Here: (A) – Primary crack initiated from borehole; (B) – Secondary crack parallel to or connected in parallel to primary crack (initiated from the primary fracture, not from the drill hole) and; (C) – Secondary crack perpendicular to the primary crack. Note that depending on the density variation, macerals are grey and minerals are white. The induced fracture network is segmented in blue, in order to clearly differentiate from the other components. (For interpretation of the references to colour in this figure legend, the reader is referred to the web version of this article.)

Fig. 9(d) shows the micro-CT image of the failed C-04 sample with the lowest break-down pressure (see Table 2). Unlike other samples, the image shows no visible grey-scale variations corresponding to phase differences, indicating that the sample has not undergone a considerable maturation (or coalification) process to develop significant amounts of minerals and maceral constituents with varying densities. This observation suggests that the particular coal type is a low rank coal, which is also in accordance with proximate analysis results. The corresponding coal type has the lowest fixed carbon content of 37.6% and ash content of 1.1% (see Fig. 5), which is a direct indication of low rank coal. The micro-CT image shows one large primary fracture initiated from the wellbore and propagated directly towards the sample surface. Although the break-down pressure is low (7.65 MPa), the induced fracture is quite extensive and wider and therefore exhibits the softer nature of the particular coal type. The results suggest that even a comparatively small pressure is enough to break-down the particular soft, low rank coal sample by creating a significant damage to the rock mass. The AE results also agree with this conclusion. Fig. 10(d) shows a large crack closure period followed by sudden uncontrolled fracture propagation of very short duration, resulting in break-down of the sample. The absence of stable fracture propagation suggests that there are no secondary fractures propagated upon the fluid injection, but the sample has failed suddenly due to the initiation of a large extensive fracture. The significant moisture content available in the sample (29.2%) creates a major contribution to this softer nature of the coal mass, because moisture loosens the bonding structure and reduces the

surface free energy of the coal mass, resulting a strength reduction [34,48]. The results suggest that the softer coals and the coal with high degree of water saturation might be subjected to irreversible damage during the hydraulic fracturing process, which might in turn result in potential contaminations of adjacent aquifers through the leaking of fracture fluid and coal seam gas.

Furthermore, the brittleness also affects the induced fracture characteristics, because high rank coal acts as brittle material and tend to induce brittle cracks during the fracturing process. More dense and thinner micro-cracks induced in brittle coal may enhance the gas extraction process with a minimal damage to the rock mass [49]. In contrast, low rank coal like specimen C-04, behaves more likely as a plastic material due to softer nature and tend to deform significantly upon mechanical loading. The excessive plastic deformation may cause extensive fracturing and irreversible damage to the reservoir [50]. The Self-healing and the CO₂ and water induced swelling effects of low rank coal may close down most of the natural and mechanically induced fractures, hindering the efficiency of gas production in the long run [51]. Coal-CO₂ interaction may trigger number of chemical reactions under favorable chemical environments, resulting in mineral dissolution/precipitation, hydrocarbon mobilization, micro-crack initiation/extension and strength alteration. These factors should also take into account, when evaluating the efficacy of CO₂-based hydraulic fracturing process in sensitive coal reservoirs. In conclusion, the heterogeneity of subsurface and the associated physical and chemical alterations in coal structure may cause a more complex fracturing process and

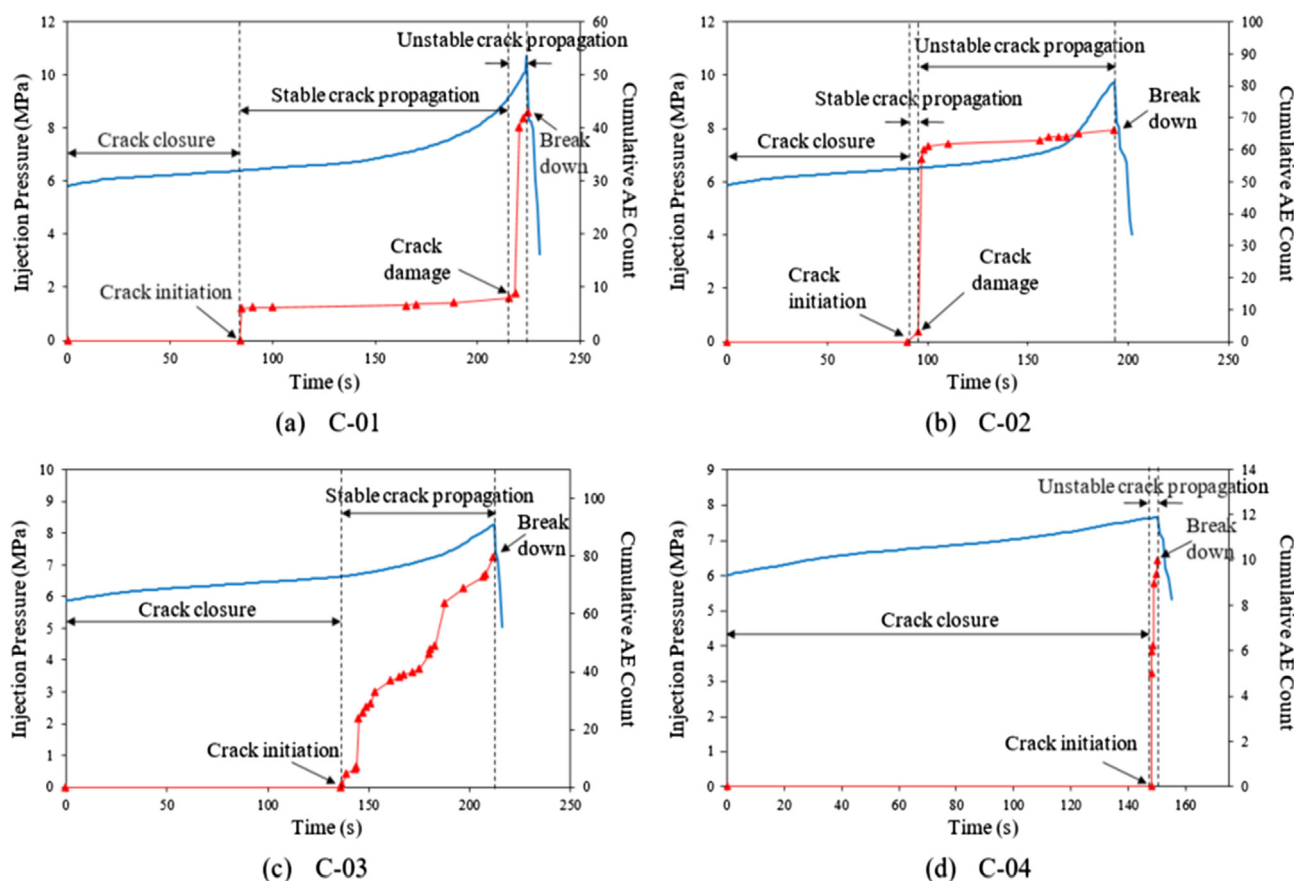


Fig. 10. Variation of cumulative acoustic emission (AE) count with time until break-down, in different coal types.

have to be assessed carefully, prior to any field stimulation project.

4. Conclusions

The efficiency and safety of hydraulic fracturing is dependent on many parameters, such as reservoir characteristics, fracturing fluid characteristics and pressurization rate, among others. Coal seams are unique rock formations that respond differently to the fracturing process, depending on the rock maturity and the composition. This study evaluates the hydraulic fracturing process using liquid CO₂ by analyzing the break-down pressure and the form of the resulting induced fracture network in various rank coal samples. The following conclusions are made:

- The break-down pressure increases with an increase in the fixed carbon content of the coal mass or coal rank. Since higher rank coal has a higher strength, this results in a higher break-down pressure. The observed non-linear trend between volatile matter content and break-down pressure implies that there is not a simple relationship between the breakdown pressure and the volatile matter content. This seems reasonable since the volatile matter content consists of a number of components, including gaseous substances and different hydrocarbons. Each of these exerts a different influence on the overall strength of the coal mass.
- The experimentally determined break-down pressure is always less than the value predicted from classical break-down theory. This is because, when using a low viscosity fluid such as liquid CO₂, the injected liquid penetrates through the interconnected pores in coal and creates an additional tangential stress in compression, which is often omitted in break-down theories. This additional stress component contributes in exerting additional pressure on the rock mass and resulting in a lower break-down pressure.

- The characteristics of the induced fracture network can be varied greatly according to the coal type and its composition. The liquid CO₂ injection induces fractures that propagate along the mineral grain boundaries, which are considered to be the weakest paths in most coal types. However, the excessive heterogeneity introduced by the complex distribution of mineral phases can cause distributed weak areas, resulting in a well distributed fracture network.
- For low rank coal, hydraulic fracturing might not be feasible, because the fracturing process fails to create a significant fracture network. Since the rock formation is considerably weakened due to the lower fixed carbon content and high moisture content, sudden break-down at low injection pressures is expected, where the resulting extensive fractures can result in risks of leakage and possible damage to coal formations and adjacent aquifers.

Thus, the results suggest that the design parameters for coal seam hydraulic fracturing, such as pressurization rate and applied techniques should carefully be evaluated while considering the characteristics of the target coal seam to enhance the gas extraction while minimizing possible reservoir damage.

References

- [1] Mariann LS, Senjen R. Hydraulic fracturing in coal seam gas mining: the risks to our health, communities, environment and climate. National Toxics Network; 2011. Briefing paper.
- [2] Sampath KHSM, Perera MSA, Ranjith PG, Matthai SK, Rathnaweera T, Zhang G, et al. CH₄-CO₂ gas exchange and supercritical CO₂ based hydraulic fracturing as CBM production-accelerating techniques a review. *J CO₂ Util* 2017;22:212–30.
- [3] Gandossi L. An overview of hydraulic fracturing and other formation stimulation technologies for shale gas production. European Commission Joint Research Centre (JRC) Technical Reports EUR 26347 EN; 2013.
- [4] Li X, Feng Z, Han G, Elsworth D, Marone C, Saffer D. Hydraulic fracturing in shale with H₂O, CO₂ and N₂, in 49th US Rock Mechanics/Geomechanics Symposium,

- American Rock Mechanics Association; 2015.
- [5] Schein G. The application and technology of slickwater fracturing. *Soc Petrol Eng* 2005.
- [6] Middleton RS, Carey JW, Currier RP, Hyman JD, Kang Q, Karra S, et al. Shale gas and non-aqueous fracturing fluids: opportunities and challenges for supercritical CO₂. *Appl Energy* 2015;147:500–9.
- [7] Alpern J, Marone C, Elsworth D, Belmonte A, Connelly P. Exploring the physico-chemical processes that govern hydraulic fracture through laboratory experiments. 46th US Symposium on Rock Mechanics and Geomechanics. 2012.
- [8] Liao S, Brunner F, Mattar L. Impact of ignoring CO₂ injection volumes on post-frac PTA. Canadian International Petroleum Conference. Petroleum Society of Canada; 2009.
- [9] Dahaghi, Kalantari A. Numerical, simulation and modeling of enhanced gas recovery and CO₂ sequestration in shale gas reservoirs: a feasibility study. SPE international conference on CO₂ capture, storage, and utilization. Society of Petroleum Engineers; 2010.
- [10] Wright CA, Tanigawa JJ, Shixin M, Li Z. Enhanced hydraulic fracture technology for a coal seam reservoir in Central China. International Meeting on Petroleum Engineering. Society of Petroleum Engineers; 2015.
- [11] Wood Harry G, Kehn TM, Carter MD, Culbertson WC. Coal resource classification system of the US Geological Survey. US Department of the Interior, Geological Survey; 1983.
- [12] Zhu Q. Coal sampling and analysis standards. London, United Kingdom: IEA Clean Coal Centre; 2014.
- [13] Donahue C-J, Rais EA. Proximate analysis of coal. *J Chem Educ* 2009;86(2):222–4.
- [14] Petrakis L, Grandy DW. Coal analysis, characterization and petrography. *J Chem Educ* 1980;57(10):689–94.
- [15] Schobert HH. The geochemistry of coal. Part I. The classification and origin of coal. *J Chem Educ* 1989;66(3):242–4.
- [16] Alpern B, De Sousa ML, Flores D. A progress report on the Alpern Coal Classification. *Int J Coal Geol* 1989;13(1–4):1–19.
- [17] Berkowitz N. An introduction to coal technology. Elsevier; 2012.
- [18] Hubbert MK, Willis DG. Mechanics of hydraulic fracturing. *Trans Am Inst Min Metall Eng* 1957;210(6):153–63.
- [19] Haimson B, Fairhurst C. Initiation and extension of hydraulic fractures in rocks. *Soc Petrol Eng J* 1967;7(3):310–8.
- [20] Ito T, Hayashi K. Physical background to the breakdown pressure in hydraulic fracturing tectonic stress measurements. *Int J Rock Mech Min Sci Geomech Abstr* 1991;28(4):285–93.
- [21] Callanan MJ. Hydraulic fracture initiation by shear failure in formations at great depths. Proc. Workshop on hydraulic fracturing stress measurements, Monterey, CA. 1981. p. 181–9.
- [22] Haimson BC, Zhao Z. Effect of borehole size and pressurization rate on hydraulic fracturing breakdown pressure. The 32nd US Symposium on Rock Mechanics (USRMS). American Rock Mechanics Association; 1991.
- [23] Schmitt DR, Zoback MD. Diminished pore pressure in low-porosity crystalline rock under tensional failure: apparent strengthening by dilatancy. *J Geophys Res Solid Earth* 1992;97(B1):273–88.
- [24] Schmitt DR, Zoback MD. Poroelastic effects in the determination of the maximum horizontal principal stress in hydraulic fracturing tests—a proposed breakdown equation employing a modified effective stress relation for tensile failure. *Int J Rock Mech Min Sci Geomech Abstr* 1989;26(6):499–506.
- [25] Li X, Feng Z, Han G, Elsworth D, Marone C, Saffer D, et al. Breakdown pressure and fracture surface morphology of hydraulic fracturing in shale with H₂O, CO₂ and N₂. *Geomech Geophys Geo-Energy Geo-Resour* 2016;2(2):63–76.
- [26] Ishida T, Chen Y, Bennour Z, Yamashita H, Inui Shuhei, Nagaya Y, et al. Features of CO₂ fracturing deduced from acoustic emission and microscopy in laboratory experiments. *J Geophys Res: Solid Earth* 2016;121(11):8080–98.
- [27] Eshiet KH, Sheng Y. Carbon dioxide injection and associated hydraulic fracturing of reservoir formations. *Environ Earth Sci* 2014;72(04):1011–24.
- [28] Middleton R, Viswanathan H, Currier R, Gupta R. CO₂ as a fracturing fluid: potential for commercial-scale shale gas production and CO₂ sequestration. *Energy Proc* 2014;63:7780–4.
- [29] Zhou X, Burbey TJ. Fluid effect on hydraulic fracture propagation behavior: a comparison between water and supercritical CO₂-like fluid. *Geofluids* 2014;14(2):174–88.
- [30] Gan Q, Elsworth D, Alpern JS, Marone C, Connolly P. Breakdown pressures due to infiltration and exclusion in finite length boreholes. *J Petrol Sci Eng* 2015;127:329–37.
- [31] Pan Z, Connell LD. A theoretical model for gas adsorption-induced coal swelling. *Int J Coal Geol* 2007;69(4):243–52.
- [32] Perera MSA, Ranjith PG, Viete DR. Effects of gaseous and super-critical carbon dioxide saturation on the mechanical properties of bituminous coal from the Southern Sydney Basin. *Appl Energy* 2013;110:73–81.
- [33] Ranjith PG, Fourar M, Pong SF, Chian W, Haque A. Characterisation of fractured rocks under uniaxial loading states. *Int J Rock Mech Min Sci Geomech* 2004;41:43–8.
- [34] Brady BH, Brown ET. Rock, mechanics: for underground mining. Springer Science & Business Media; 2013.
- [35] Vishal V, Ranjith PG, Singh TN. An experimental investigation on behaviour of coal under fluid saturation, using acoustic emission. *J Nat Gas Sci Eng* 2015;22:428–36.
- [36] Zhang Y, Lebedev M, Al-Yaseri A, Yu H, Xu X, Sarmadivaleh M, et al. Nanoscale rock mechanical property changes in heterogeneous coal after water adsorption. *Fuel* 2018;218:23–32.
- [37] Zhang X, Lu Y, Tang J, Zhou Z, Liao Y. Experimental study on fracture initiation and propagation in shale using supercritical carbon dioxide fracturing. *Fuel* 2017;190:370–8.
- [38] Hou P, Gao F, Ju Y, Yang Y, Gao Y, Liu J. Effect of water and nitrogen fracturing fluids on initiation and extension of fracture in hydraulic fracturing of porous rock. *J Nat Gas Sci Eng* 2017;45:38–52.
- [39] Kang SM, Fathi E, Ambrose RJ. Carbon dioxide storage capacity of organic-rich shales. *Soc Petrol Eng J* 2011;16:842–55.
- [40] Zhang X, Wang JG, Gao F, Ju Y. Impact of water, nitrogen and CO₂ fracturing fluids on fracturing initiation pressure and flow pattern in anisotropic shale reservoirs. *J Nat Gas Sci Eng* 2017;45:291–306.
- [41] Carlson WD, Rowe T, Ketcham RA, Colbert MW. Applications of high-resolution X-ray computed tomography in petrology, meteoritics and palaeontology. *Geol Soc London, Spec Publ* 2003;215(1):7–22.
- [42] Ramandi HL, Armstrong RT, Mostaghimi P. Micro-CT image calibration to improve fracture aperture measurement. *Case Stud NondestrTest Eval* 2016;6:4–13.
- [43] Ramandi HL, Mostaghimi P, Armstrong RT. Digital rock analysis for accurate prediction of fractured media permeability. *J Hydrol* 2017;554:817–26.
- [44] Eberhardt E, Stead D, Stimpson B. Quantifying progressive pre-peak brittle fracture damage in rock during uniaxial compression. *Int J Rock Mech Min Sci Geomech* 1999;36(3):361–80.
- [45] Ishida T, Aoyagi K, Niwa T, Chen Y, Murata S, Chen Q, et al. Acoustic emission monitoring of hydraulic fracturing laboratory experiment with supercritical and liquid CO₂. *Geophys Res Lett* 2012;39:1–6.
- [46] Amann F, Ündül Ö, Kaiser PK. Crack initiation and crack propagation in heterogeneous sulfate-rich clay rocks. *Rock Mech Rock Eng* 2014;47(5):1849–65.
- [47] Ündül Ö, Amann F, Aysal N, Plötze ML. Micro-textural effects on crack initiation and crack propagation of andesitic rocks. *Eng Geol* 2015;193:267–75.
- [48] Lama RD, Vutukuri VS. Handbook on mechanical properties of rocks-testing techniques and results. 1978. p. 2.
- [49] Bieniawski ZT. Propagation of brittle fracture in rock. 10th US Symposium on Rock Mechanics (USRMS). American Rock Mechanics Association; 1968.
- [50] Sampath KHSM, Perera MSA, Elsworth D, Ranjith PG, Matthai SK, Rathnaweera T. Experimental investigation on the mechanical behavior of victorian brown coal under brine saturation. *Energy Fuels* 2018;32(5):5799–811.
- [51] Mazumder S, Karnik A, Wolf K-H. Swelling of coal in response to CO₂ sequestration for ECBM and its effect on fracture permeability. *SPE J* 2006;11(3):390–8.